Ionics (2020) 26:711–717
https://doi.org/10.1007/s11581-019-03235-7

ORIGINAL PAPER

Facile synthesis of hybrid MoS_2/graphene nanosheets as high-performance anode for sodium-ion batteries

Rong Zhang[1] · Jinkai Wang[1] · Chao Li[2] · Ting Liu[1] · Tianhao Yao[1] · Lei Zhu[1] · Xiaogang Han[1] · Hongkang Wang[1,2]

Received: 3 July 2019 / Revised: 3 August 2019 / Accepted: 23 August 2019 / Published online: 31 August 2019
© Springer-Verlag GmbH Germany, part of Springer Nature 2019

Abstract

We report the facile synthesis of molybdenum disulfide (MoS_2) nanosheets on graphene nanosheets (MoS_2@GNSs) via simple thermal decomposition of ammonium tetrathiomolybdate in Ar-H_2 atmosphere. When used as anode materials for sodium-ion batteries (SIBs), the as-prepared MoS_2@GNSs electrode delivers reversible capacities of 389 and 383 mA h g^{-1} at current densities of 200 mA g^{-1} and 500 mA g^{-1} after 200 cycles, respectively, which is much higher than that of the MoS_2 electrode (253 mA h g^{-1} after 171 cycles at 200 mA g^{-1}). The superior sodium storage performance of MoS_2@GNSs including excellent cycle stability and rate performance can be attributed to the introduction of graphene materials, which not only buffer the volume changes of MoS_2 upon sodiation/desodiation but also improve the electrical conductivity.

Keywords MoS_2 · Graphene · Pyrolysis · Sodium-ion batteries

Sodium-ion batteries (SIBs) are attracting increasing interest and have been considered as a promising alternative for the currently widely used lithium-ion batteries (LIBs) [1–4], owing to the abundant and inexpensive sodium resources on earth. Even though SIBs show similar working mechanism with that of the LIBs, the current SIBs usually exhibit slower reaction kinetics, low specific capacity, and poor cycle life because of the large ionic radius of Na^+ (ca. 1.02 Å) than that of Li^+ (ca. 0.76 Å), and the heavier molar mass of Na^+ (22.99 g mol^{-1}) than that of Li^+ (6.94 g mol^{-1}) [5, 6]. Therefore, the ongoing researches on SIBs are mainly focusing on exploring novel electrode materials with higher sodium storage capacity and better cycling behavior, and metal sulfides with a high theoretical specific capacity have been considered as promising anodes for rechargeable SIBs [7–9].

Among various candidate anode materials for SIBs, MoS_2 has attracted considerable attentions as a high-performance potential anode material for SIBs due to its layered structure and high theoretical capacity of 670 mA h g^{-1} [10–13]. Notably, MoS_2 possesses a relatively wide interlayer structure, which is beneficial for fast Na^+ insertion/extraction [14–17]. However, because of the low electronic conductivity and serious volume expansion of MoS_2 during sodiation, the battery usually displays low specific capacity and poor cycling stability, which makes it extremely challenging in practical applications [18]. To solve this problem, a common and effective method is to combine MoS_2 with a conductive carbonaceous material. For example, Bang et al. reported the synthesis of liquid-phase exfoliated MoS_2 nanosheets, delivering a discharge capacity of 165 mA h g^{-1} after 50 cycles at a current density of 20 mA g^{-1}, when hybridized with rGO as anode for SIBs [19–21]. Yang et al. reported the synthesis of MoS_2/graphite composite for SIBs which displayed a high reversible capacity of 358.2 mA h g^{-1} at 100 mA g^{-1} [22]. Kong et al. reported MoS_2/graphene paper which can provide a capacity of 76.8 mA h g^{-1} after 300 cycles at 100 mA g^{-1} [23]. Chen et al. synthesized MoS_2 /carbon nanofibers and the electrode showed discharge capacities of 380 mA h g^{-1} after 50 cycles at 50 mA g^{-1} [24, 25].

Electronic supplementary material The online version of this article (https://doi.org/10.1007/s11581-019-03235-7) contains supplementary material, which is available to authorized users.

✉ Hongkang Wang
hongkang.wang@mail.xjtu.edu.cn

[1] State Key Lab of Electrical Insulation and Power Equipment, Center of Nanomaterials for Renewable Energy (CNRE), School of Electrical Engineering, Xi'an Jiaotong University, Xi'an 710049, People's Republic of China

[2] Xi'an Key Laboratory of Sustainable Energy Material Chemistry, and Instrument Analysis Center, Xi'an Jiaotong University, Xi'an 710049, China

However, due to the high cost and complexity of these sample preparation processes, these methods are still difficult for large scale applications. This has inspired us to design and develop a facile and low-cost synthesis process to improve the sodium-ion storage characteristics of MoS_2. Herein, MoS_2@GNSs with unique structure and excellent electrochemical performance is designed and manufactured by a facile and low-cost method, namely, via a simple thermal decomposition of ammonium tetrathiomolybdate with the presence of graphene nanosheets.

Experimental section

Material synthesis

For synthesis of MoS_2, 0.2 g of ammonium tetrathiomolybdate ($(NH_4)_2MoS_4$, J&K Scientific) was placed in a tube furnace and annealed at 800 °C for 2 h in mixed Ar-H_2 (10% H_2+ 90% Ar) at a heating rate of 10 °C min^{-1}. In the typical synthesis of MoS_2@GNSs, 5 mg of graphene nanosheets (GNSs) and 0.1 g of ammonium tetrathiomolybdate were mixed/dissolved in 4 mL of N, N-dimethylformamide (DMF, C_3H_7NO, Shanghai Macklin Biochemical) under ultrasound irradiation for 2 h, and then the solution was transferred and kept in an oven at 100 °C for 1 h, in order to completely evaporate the DMF. Thus, obtained black product was annealed at 800 °C for 2 h under the same condition.

Material characterization

The phase structure of the products were characterized by X-ray diffraction (XRD) analysis under Cu K a radiation (k = 1.5418 Å) at 30 kV and 10 mA in the range of 10–80°. Scanning electron microscopy (SEM) was carried out with Quanta 250F FEI SEM. Transmission electron microscopy (TEM) was performed with JEOL-2100 TEM operated at 200 kV. Thermogravimetric analysis (TGA) was performed at a heating rate of 10 °C min^{-1} in air using a Mettler Toledo Thermal Analysis TGA-DSC thermal analyzer system. The composition and chemical state of the products were recorded using a Physical Electronics PHI-5802 analysis system by X-ray photoelectron spectroscopy (XPS) with a monochromatic Al Ka X-ray source. Raman measurements were performed on a Renishaw RE01 system with an excitation wavelength of 633 nm.

Electrochemical measurements

The electrochemical properties were tested using CR2025 coin-type cell assembled in an Ar-filled glovebox where the contents of H_2O and O_2 were less than 0.1 ppm. The active materials, carbon black, and polyacrylic acid (PAA) were mixed at a weight ratio of 80:10:10 and pasted on a copper foil current collector, followed by drying under vacuum at 60 °C for 12 h. The loading of the active material was in the range of 1.0–1.2 mg cm^{-2}. The sodium foil was used as the counter electrode and a Whatman glass fiber membrane was used as the separator. The electrolyte was prepared by dissolving 1 M $NaClO_4$ in ethylene carbonate/dimethyl carbonate (EC/DMC, volume ratio 1:1) with addition of 5% of fluoroethylene carbonate (FEC) by volume. Cyclic voltammograms (CV) were performed using an electrochemical station (Autolab 302 N) with a voltage range of 0.01–3.0 V at a scan rate of 0.2 mV s^{-1}. The discharge-charge test was performed using a battery test system (Neware BTS, China) in the range of 0.01–3.0 V. Electrochemical impedance spectroscopy (EIS) was also performed using an electrochemical station in the frequency range of 10 MHz to 0.01 Hz. The specific capacity is calculated based on the composite mass of MoS_2 and MoS_2@GNSs.

Results and discussion

Figure 1a compares the X-ray diffraction (XRD) patterns of the MoS_2 and MoS_2@GNSs. Both products display almost identical diffraction profiles, and all the diffraction peaks can be indexed to the MoS_2 (JCPDS No. 65-7025), in which the prominent peaks located at 14.4°, 33.5°, 39.6°, and 58.3° can be assigned to the (002), (101), (103), and (110) planes of the MoS_2 phase. Notably, the presence of the outstanding (002) diffraction peak at 14.4° with d-spacing of ~ 0.61 nm indicates the layered crystalline structure. No peaks belonging to other materials can be observed, indicating the high purity of the product and the feasibility of producing layered MoS_2 by directly annealing $(NH_4)_2MoS_4$ under Ar-H_2 flow. To determine the graphene content in the MoS_2@GNSs composites, TGA test (Fig. 1b) was performed in the temperature ranging from 25 to 800 °C in air. The sharp weight loss at around 400 °C is attributed to the oxidation of MoS_2 to MoO_3, resulting the formation of MoO_3, while the weight loss at 400 to 500 °C is due to the oxidation of carbon to CO_2. On the basis of the following Eqs. (1–3) [26], the weight percentages of MoS_2 and graphene in the MoS_2@GNSs are calculated as 91.4% and 8.6%, which is consistent with the theoretical values.

$$2MoS_2(s) + 7O_2(g) \rightarrow 2MoO_3(s) + 4SO_2(g) \quad (1)$$

$$C + O_2 \rightarrow CO_2 \quad (2)$$

$$MoS_2(wt\%) = 100 \times \frac{M_{MoS_2}}{M_{MoO_3}} \times \frac{\text{Final weight of } MoO_3}{\text{Initial weight of } MoS_2\text{−graphene}} \quad (3)$$

The morphology and the microstructure of MoS_2 were examined by SEM and TEM. Figure 2a and b show the typical

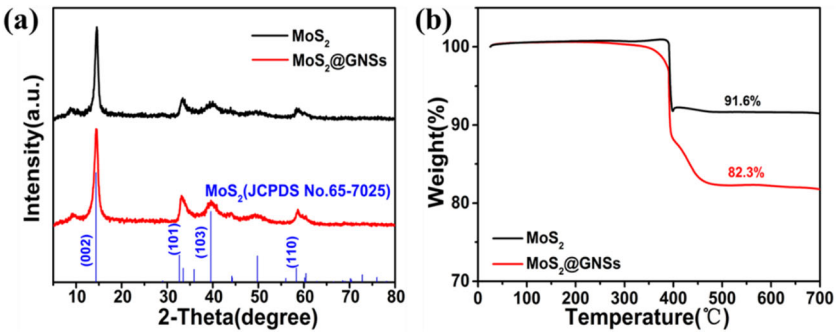

Fig. 1 **a** XRD patterns and **b** TGA curves of the MoS_2 and MoS_2@GNSs

SEM images of MoS_2, exhibiting an irregular morphology with aggregates of nanosheets. Figure 2c and d show the TEM/HRTEM images of an aggregate of MoS_2, which is composed of aligned nanosheets. Furthermore, HRTEM image clearly displays the well-defined lattice fringes with d-spacing of 0.61 nm, which can be indexed to the (002) reflection of the MoS_2 (Fig. 1d).

Figure 3a and b show the SEM images of MoS_2@GNSs which were obtained by annealing the $(NH_4)_2MoS_4$/GNSs under Ar-H_2 flow. Significantly, thinner nanosheets can be observed, as compared with the pure MoS_2 counterpart (Fig. 2a, b). As shown in the TEM image (Fig. 3c), the nanosheets are flexible to some extent. HRTEM image in Fig. 3d reveals that nanosheets are aggregated but with different orientation, and the lattice fringes with d-spacing of 0.62 nm correspond to the (002) plane of MoS_2. As revealed by HAADF-STEM image and the corresponding EDS maps, the thin MoS_2 nanosheets are standing on the graphene nanosheets. The Mo and S elemental maps are well overlapped, while the graphene nanosheets serve as a support (Fig. 3e). In addition, N-doping may happen owing to the generation of the ammonium by the decomposition of $(NH_4)_2MoS_4$.

The chemical composition and the valence state of the obtained MoS_2@GNSs were examined by X-ray photoelectron spectroscopy (XPS). Figure 4 a shows the survey XPS spectrum of the MoS_2@GNSs, revealing the presence of Mo, S, and C elements [27]. In the Mo 3d XPS spectrum (Fig. 4b), two distinct characteristic peaks at 228.7 and 231.8 eV can be attributed to the Mo $3d_{5/2}$ and Mo $3d_{3/2}$, respectively, with oxidation state of Mo^{4+}. In addition, the minor peak at 235.4 eV can be assigned to the formation of Mo^{6+}-O. The peak at 225.8 eV corresponds to S 2 s. Figure 4c shows the core level S 2p spectrum of the MoS_2@GNSs, in which the deconvolved two peaks at 161.5 and 162.7 eV correspondingly relate to the S $2p_{3/2}$ and S $2p_{1/2}$, indicating that sulfur is present as S^{2-} ions. Figure 4d depicts the overlapped N1s and Mo 3p XPS spectrum, in which the prominent peaks with binding energy at 394.7 eV corresponds to Mo $3p_{3/2}$, while

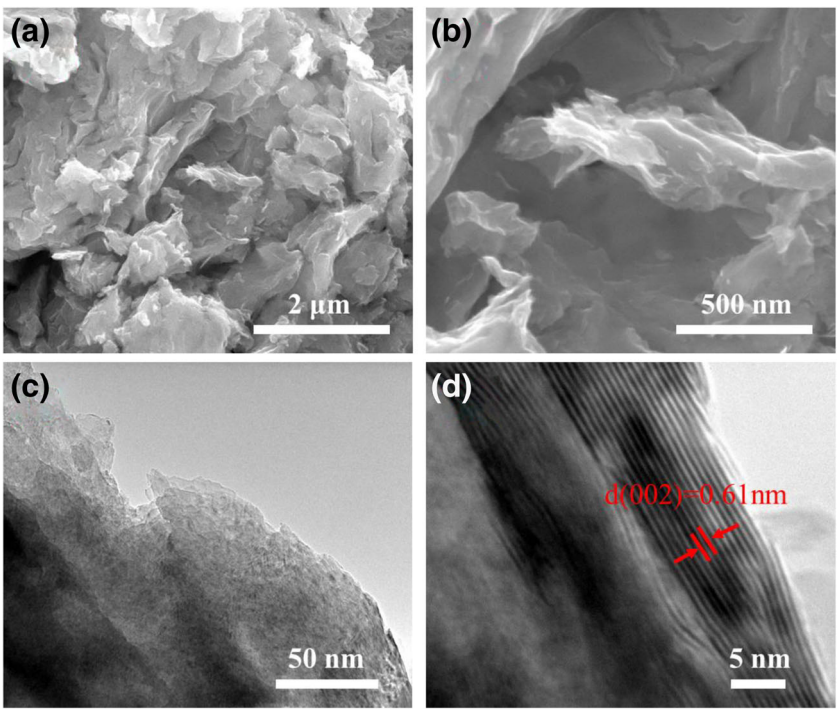

Fig. 2 **a**, **b** SEM images, **c** TEM, and **d** HRTEM images of MoS_2

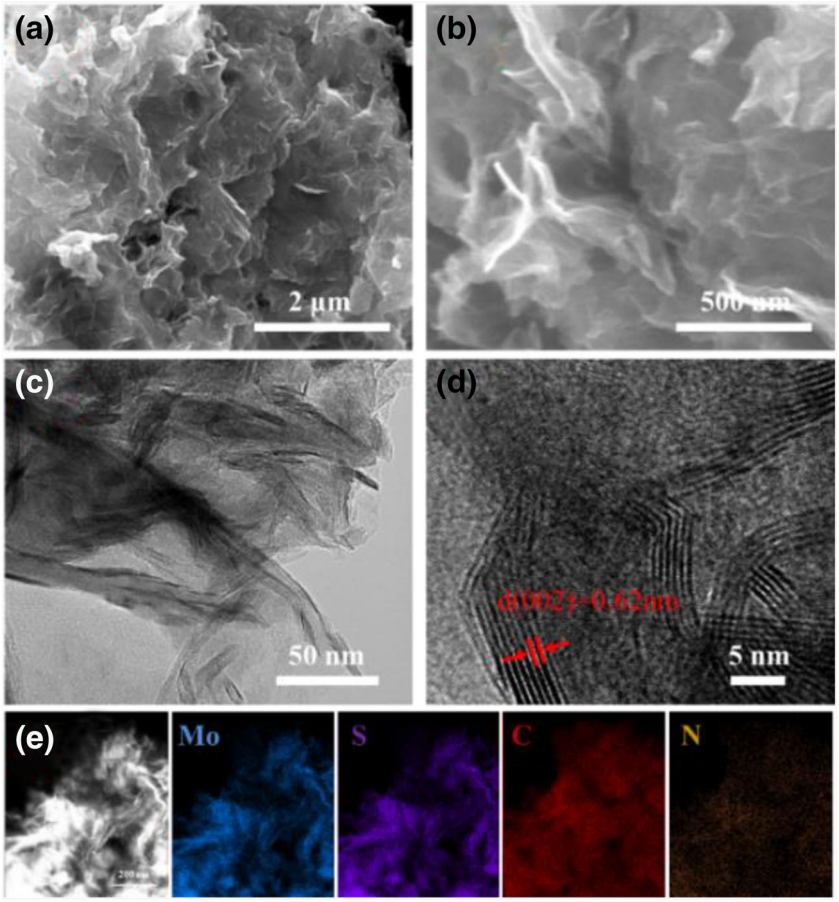

Fig. 3 **a**, **b** SEM images, **c** TEM, and **d** HRTEM images of MoS_2@GNSs. **e** STEM image and the corresponding elemental maps of Mo, S, C, and N in the MoS_2@GNSs

the peak with binding energy at 397.4 eV can be assigned to the nitride type of N atom, indicating the formation of N-Mo bond [28–30]. Raman spectrum of the MoS_2@GNSs shows two distinct peaks at about 378 and 406 cm^{-1}, corresponding to the E1 2g and A_{1g} vibration modes of MoS_2, respectively. The A_{1g} mode comes from out-of-plane vibration, while the E1 2g mode originates from the Mo-S in-plane vibration [30–32]. Besides, two broad bands at about 1326 cm^{-1}

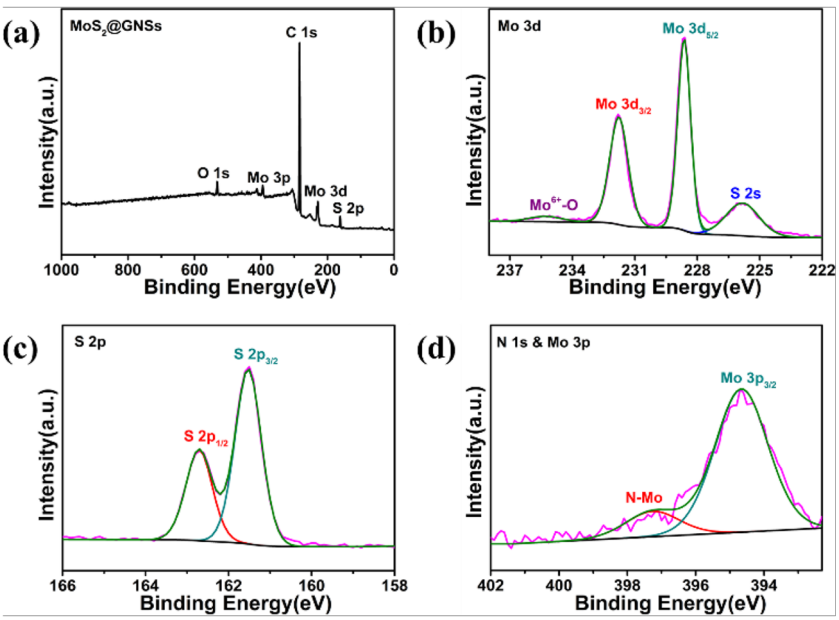

Fig. 4 XPS spectra of MoS_2@GNSs composite: **a** survey spectrum, **b** Mo 3d spectrum, **c** S 2p spectrum, **d** N 1s & Mo 3p spectrum

(disorder-induced D-band) and 1597 cm^{-1} (graphite G-band) are observed and originated from the graphene nanosheets (Figure S1) [33, 34].

The electrochemical properties of the MoS_2 and MoS_2@GNSs were examined as anode materials for SIBs using sodium foil as the reference and counter electrode. Figure 5a shows the initial five CV curves of the MoS_2@GNSs electrode at a scan rate of 0.2 mV s^{-1} in the voltage range of 0.01 to 3 V. In the first cathodic scan, a distinct reduction peak located at around 0.71 V is observed, which can be attributed to the insertion of Na^+ into the MoS_2 interlayer ($MoS_2 + xNa^+ + xe^- \rightarrow Na_xMoS_2$) and formation of a solid electrolyte interphase (SEI) layer [35–37]. In the anodic scan, the broad peak at 1.85 V can be attributed to the oxidation of metallic Mo to MoS_2. Since the second CV onwards, the prominent anode and cathode peaks are changed a little and locate at approximately 1.77 and 0.76 V, respectively. Except for the first cycle, the CV curves overlap well in the profile, which reflects the high reversibility and good cycle stability of MoS_2@GNSs.

Figure 5b presents the discharge and charge voltage profiles of the MoS_2@GNSs electrode at the 1st, 2nd, 10th, 50th, 100th, and 150th cycles at a current density of 0.5 A g^{-1}. The initial discharge and charge capacities of the MoS_2@GNSs composite are 526.4 and 374.7 mA h g^{-1}, respectively, displaying a columbic efficiency of 71.2%. The irreversible capacity loss and thus resulting low columbic efficiency is attributed to the irreversible formation of the SEI layer on the surface of the electrode [38–40]. Surprisingly, the reversible capacity of 343 at the 2nd cycle increases to 380 mA h g^{-1} after 150 cycles, with a columbic efficiency as high as 97.3%. This indicates that the MoS_2@GNSs electrode provides a stable capacity at a current density of 0.5 A g^{-1}, implying high capacity and good reversibility.

Figure 5c compares the cycling performance of the MoS_2 and MoS_2@GNSs electrodes at a current density of 0.2 and 0.5 A g^{-1}. Although the initial capacity of the MoS_2@GNSs electrode is lower than that of MoS_2, and both MoS_2 and MoS_2@GNSs electrodes show increasing capacities with cycle number increasing to 130, the MoS_2 electrodes show abrupt fast capacity fading, which may be due to the electrode pulverization upon cycling. Notably, the MoS_2@GNSs electrodes show stable cycle performance, delivering reversible capacities of 389 and 383 mA h g^{-1} after 200 cycles at current densities of 0.2 and 0.5 A g^{-1}, respectively. Furthermore, the rate performance of the MoS_2@GNSs electrode is shown in Fig. 5d, and the MoS_2@GNSs electrode exhibits discharge capacities of 377, 370, 354, 334, 308, and 267 mA h g^{-1} each after 10 cycles at successively increased current densities from 0.1, 0.2, 0.5, 1, 2 to even 5 A g^{-1}, respectively. When the current density is back to 0.1 A g^{-1}, the MoS_2@GNSs electrode shows a high reversible capacity of 398 mA h g^{-1}, indicating the superior rate capability of the MoS_2@GNSs electrode. The excellent sodium-ion storage properties of the MoS_2/GNSs composite can be attributed to the efficient hybridization of the few-layer MoS_2 nanosheets with expanded d-spacing and the continuous graphene nanosheet networks. First, the reduced stacking of MoS_2 nanosheets can relax partial strain, and the larger d-spacing can lower the barrier for Na^+ insertion. Second, the dispersion of MoS_2 nanosheets by the graphene nanosheets facilitates the Na^+ accessibility into reaction sites and the infiltration of electrolyte during cycling.

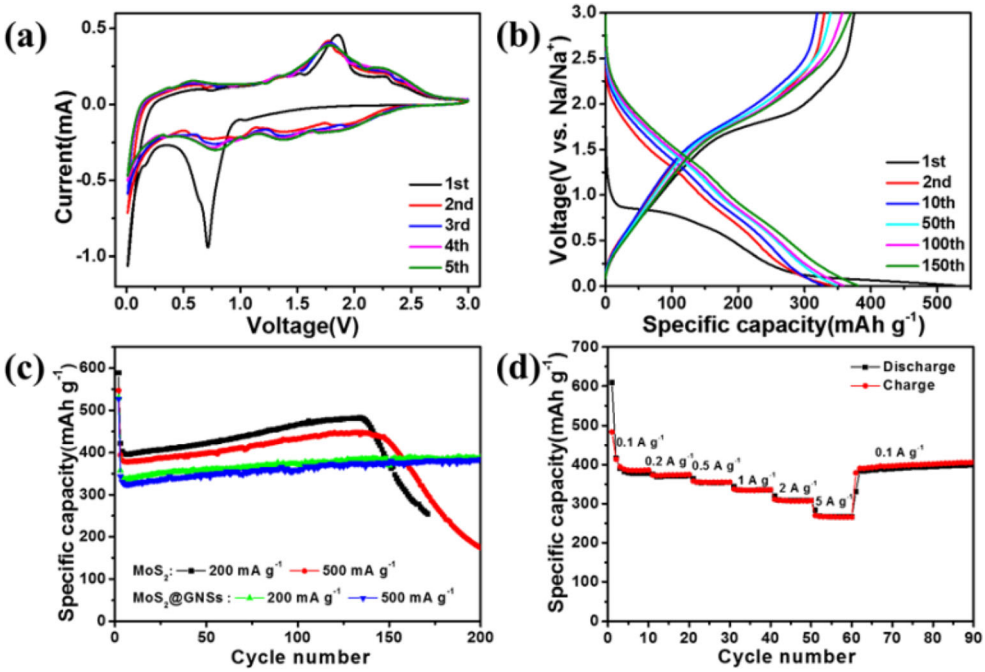

Fig. 5 **a** Cyclic voltammetry (CV) curves of the MoS_2@GNSs electrode at a scan rate of 0.2 mV s^{-1}. **b** Discharge/charge profiles of the MoS_2@GNSs electrode at a current density of 0.5 A g^{-1}. **c** Cycling performance of the MoS_2 and MoS_2@GNSs electrodes. **d** Rate capability of the MoS_2@GNSs electrodes

Third, the flexible graphene nanosheets not only offer cushions to relieve volume expansion but also enhance the electrical conductivity of the composite.

Conclusions

In summary, a hybrid of MoS_2@GNSs with MoS_2 nanosheets grown on graphene nanosheets (GNSs) has been successfully prepared by a facile pyrolysis of ammonium tetrathiomolybdate-GNSs. Owing to the introduction of GNSs, thinner MoS_2 nanosheets were obtained and readily grown on the GNSs. When examined as anode materials for sodium-ion batteries, MoS_2@GNSs electrode delivered high reversible capacity of 383 mA h g^{-1} after 200 cycles at 0.5 A g^{-1}, demonstrating high sodium storage capacity, superior cycle stability, and rate capability. More importantly, this work provided a new simplified route for synthesis of MoS_2 based anode materials for high-performance SIB materials, which can be expected for various applications in the field of electrochemical energy storage and conversion.

Acknowledgments We thank Mr. Chuansheng Ma and Ms. Yanzhu Dai at International Center for Dielectric Research (ICDR) of Xi'an Jiaotong University for the help with TEM/SEM measurements.

Funding information This work was supported by the Natural Science Basis Research Plan in Shaanxi Province of China (No. 2018JM5085) and the Key Laboratory Construction Program of Xi'an Municipal Bureau of Science and Technology (201805056ZD7CG40). H.W. appreciates the support of the Tang Scholar Program from the Cyrus Tang Foundation

References

1. Kim S-W, Seo D-H, Ma X, Ceder G, Kang K (2012) Electrode materials for rechargeable sodium-ion batteries: potential alternatives to current lithium-ion batteries. Adv Energy Mater 2:710–721
2. Cao Y, Xiao L, Wang W, Choi D, Nie Z, Yu J, Saraf LV, Yang Z, Liu J (2011) Reversible sodium ion insertion in single crystalline manganese oxide nanowires with long cycle life. Adv Mater 23:3155–3160
3. Lu X, Wang Z, Liu K, Luo J, Wang P, Niu C, Wang H, Li W (2019) Hierarchical Sb_2MoO_6 microspheres for high-performance sodium-ion battery anode. Energy Storage Mater 17:101–110
4. Wang J, Cao D, Yang G, Yang Y, Wang H (2017) Synthesis of nis/carbon composites as anodes for high-performance sodium-ion batteries. J Solid State Electrochem 21:3047–3055
5. Park Y-U, Seo D-H, Kwon H-S, Kim B, Kim J, Kim H, Kim I, Yoo H-I, Kang K (2013) A new high-energy cathode for a na-ion battery with ultrahigh stability. J Am Chem Soc 135:13870–13878
6. Chevrier VL, Ceder G (2011) Challenges for na-ion negative electrodes. J Electrochem Soc 158:A1011–A1014
7. Zhang N, Han X, Liu Y, Hu X, Zhao Q, Chen J (2015) 3D porous gamma-Fe_2O_3@C nanocomposite as high-performance anode material of na-ion batteries. Adv Energy Mater 5:1401123
8. Zhou T, Pang WK, Zhang C, Yang J, Chen Z, Liu HK, Guo Z (2014) Enhanced sodium-ion battery performance by structural phase transition from two-dimensional hexagonal-SnS_2 to orthorhombic-SnS. ACS Nano 8:8323–8333
9. Xu J, Zhang J, Zhang W, Lee C-S (2017) Interlayer nanoarchitectonics of two-dimensional transition-metal dichalcogenides nanosheets for energy storage and conversion applications. Adv Energy Mater 7:1700571
10. Huang X, Zeng Z, Zhang H (2013) Metal dichalcogenide nanosheets: preparation, properties and applications. Chem Soc Rev 42:1934–1946
11. Hu X, Zhang W, Liu X, Mei Y, Huang Y (2015) Nanostructured mo-based electrode materials for electrochemical energy storage. Chem Soc Rev 44:2376–2404
12. Balendhran S, Walia S, Nili H, Ou JZ, Zhuiykov S, Kaner RB, Sriram S, Bhaskaran M, Kalantar-zadeh K (2013) Two-dimensional molybdenum trioxide and dichalcogenides. Adv Funct Mater 23:3952–3970
13. Kang W, Wang Y, Xu J (2017) Recent progress in layered metal dichalcogenide nanostructures as electrodes for high-performance sodium-ion batteries. J Mater Chem A 5:7667–7690
14. Su D, Dou S, Wang G (2015) Ultrathin MoS_2 nanosheets as anode materials for sodium-ion batteries with superior performance. Adv Energy Mater 5:1401205
15. Tan C, Zhang H (2015) Two-dimensional transition metal dichalcogenide nanosheet-based composites. Chem Soc Rev 44:2713–2731
16. Chhowalla M, Shin HS, Eda G, Li L-J, Loh KP, Zhang H (2013) The chemistry of two-dimensional layered transition metal dichalcogenide nanosheets. Nat Chem 5:263–275
17. Zhang J, Wu M, Liu T, Kang W, Xu J (2017) Hierarchical nanotubes constructed from interlayer-expanded $MoSe_2$ nanosheets as a highly durable electrode for sodium storage. J Mater Chem A 5:24859–24866
18. Wang X, Li Y, Guan Z, Wang Z, Chen L (2015) Micro-MoS_2 with excellent reversible sodium-ion storage. Chem Europ J 21:6465–6468
19. Bang GS, Nam KW, Kim JY, Shin J, Choi JW, Choi S-Y (2014) Effective liquid-phase exfoliation and sodium ion battery application of MoS_2 nanosheets. ACS Appl Mater Interfaces 6:7084–7089
20. You Y, Ye Y, Wei M, Sun W, Tang Q, Zhang J, Chen X, Li H, Xu J (2019) Three-dimensional MoS_2/rGo foams as efficient sulfur hosts for high-performance lithium-sulfur batteries. Chem Eng J 355:671–678
21. Ren W, Zhou W, Zhang H, Cheng C (2017) Ald TiO_2-coated flower-like MoS_2 nanosheets on carbon cloth as sodium ion battery anode with enhanced cycling stability and rate capability. ACS Appl Mater Interfaces 9:487–495
22. Yang Q, Liu M, Hu Y, Xu Y, Kong L, Kang L (2018) Facile synthesis of MoS_2/graphite intercalated composite with enhanced electrochemical performance for sodium ion battery. J Energy Chem 27:1208–1213
23. Kong D, Cheng C, Wang Y, Huang Z, Liu B, Von Lim Y, Ge Q, Yang HY (2017) Fe_3O4 quantum dot decorated MoS_2 nanosheet arrays on graphite paper as free-standing sodium-ion battery anodes. J Mater Chem A 5:9122–9131
24. Chen C, Li G, Lu Y, Zhu J, Jiang M, Hu Y, Cao L, Zhang X (2016) Chemical vapor deposited MoS_2/electrospun carbon nanofiber composite as anode material for high-performance sodium-ion batteries. Electrochim Acta 222:1751–1760
25. Hou J, Cao T, Idrees F, Cao C (2016) A co-sol-emulsion-gel synthesis of tunable and uniform hollow carbon nanospheres with interconnected mesoporous shells. Nanoscale 8:451–457
26. Wang J, Luo C, Gao T, Langrock A, Mignerey AC, Wang C (2015) An advanced MoS_2/carbon anode for high-performance sodium-ion batteries. Small 11:473–481

27. Zuo X, Chang K, Zhao J, Xie Z, Tang H, Li B, Chang Z (2016) Bubble-template-assisted synthesis of hollow fullerene-like MoS_2 nanocages as a lithium ion battery anode material. J Mater Chem A 4:51–58
28. Teng Y, Zhao H, Zhang Z, Zhao L, Zhang Y, Li Z, Xia Q, Du Z, Świerczek K (2017) MoS_2 nanosheets vertically grown on reduced graphene oxide via oxygen bonds with carbon coating as ultrafast sodium ion batteries anodes. Carbon 119:91–100
29. Hou J, Cao C, Idrees F, Ma X (2015) Hierarchical porous nitrogen-doped carbon nanosheets derived from silk for ultrahigh-capacity battery anodes and supercapacitors. ACS Nano 9:2556–2564
30. Zhang J, Kang W, Jiang M, You Y, Cao Y, Ng TW, Yu DY, Lee CS, Xu J (2017) Conversion of 1T-$MoSe_2$ to 2H-MoS_2xSe_2-2x mesoporous nanospheres for superior sodium storage performance. Nanoscale 9:1484–1490
31. Kong D, Wang H, Cha JJ, Pasta M, Koski KJ, Yao J, Cui Y (2013) Synthesis of MoS_2 and $MoSe_2$ films with vertically aligned layers. Nano Lett 13:1341–1347
32. Cao X, Shi Y, Shi W, Rui X, Yan Q, Kong J, Zhang H (2013) Preparation of MoS_2-coated three-dimensional graphene networks for high-performance anode material in lithium-ion batteries. Small 9:3433–3438
33. Hou J, Jiang K, Wei R, Tahir M, Wu X, Shen M, Wang X, Cao C (2017) Popcorn-derived porous carbon flakes with an ultrahigh specific surface area for superior performance supercapacitors. ACS Appl Mater Interfaces 9:30626–30634
34. Ren W, Zhang H, Guan C, Cheng C (2017) Ultrathin MoS_2 nanosheets@metal organic framework-derived n-doped carbon nanowall arrays as sodium ion battery anode with superior cycling life and rate capability. Adv Funct Mater 27:1702116
35. Lu Y, Zhao Q, Zhang N, Lei K, Li F, Chen J (2016) Facile spraying synthesis and high-performance sodium storage of mesoporous MoS_2/C microspheres. Adv Funct Mater 26:911–918
36. Lacey SD, Wan J, Cresce AW, Russell SM, Dai J, Bao W, Xu K, Hu L (2015) Atomic force microscopy studies on molybdenum disulfide flakes as sodium-ion anodes. Nano Lett 15:1018–1024
37. Hou J, Jiang K, Tahir M, Wu X, Idrees F, Shen M, Cao C (2017) Tunable porous structure of carbon nanosheets derived from puffed rice for high energy density supercapacitors. J Power Sources 371: 148–155
38. Xu M, Yi F, Niu Y, Xie J, Hou J, Liu S, Hu W, Li Y, Li CM (2015) Solvent-mediated directionally self-assembling MoS_2 nanosheets into a novel worm-like structure and its application in sodium batteries. J Mater Chem A 3:9932–9937
39. Qin W, Chen T, Pan L, Niu L, Hu B, Li D, Li J, Sun Z (2015) MoS_2-reduced graphene oxide composites via microwave assisted synthesis for sodium ion battery anode with improved capacity and cycling performance. Electrochim Acta 153:55–61
40. Shi Z-T, Kang W, Xu J, Sun L-L, Wu C, Wang L, Yu Y-Q, Yu DYW, Zhang W, Lee C-S (2015) In situ carbon-doped $Mo(Se_{0.85}S_{0.15})_2$ hierarchical nanotubes as stable anodes for high-performance sodium-ion batteries. Small 11:5667–5674

Publisher's note Springer Nature remains neutral with regard to jurisdictional claims in published maps and institutional affiliations.